ACS APPLIED MATERIALS & INTERFACES

Research Article

www.acsami.org

Series of New D-A-π-A Organic Broadly Absorbing Sensitizers Containing Isoindigo Unit for Highly Efficient Dye-Sensitized Solar Cells

Weijiang Ying,[†] Fuling Guo,[†] Jing Li, Qiong Zhang, Wenjun Wu, He Tian, and Jianli Hua*

Key Laboratory for Advanced Materials and Institute of Fine Chemicals, East China University of Science and Technology, Shanghai 200237, P.R. China

ABSTRACT: In this work, six new D-A-π-A sensitizers (**ID1**−**ID6**), with triarylamine as the electron donor; isoindigo as a auxiliary electron withdrawing unit; thiophene, furan, and benzene as the linker; and cyanoacrylic acid as the anchoring group, were synthesized through simple synthetic procedures and with low cost. Their absorption spectra were broad with long wavelength absorption maximum approximately at 589 nm and the absorption onset at 720 nm on the TiO_2 film. Electrochemical experiments indicate that the HOMO and LUMO energy levels can be conveniently tuned by alternating the donor moiety and the linker. All of these dyes performed as sensitizers for the DSSCs test under AM 1.5 similar experimental conditions, and a maximum overall conversion efficiency of 5.98% (J_{sc} = 14.77 mA cm^{-2}, V_{oc} = 644 mV, ff = 0.63) is obtained for **ID6**-based DSSCs when TiO_2 films were first immersed for 6 h in 20 mM CDCA ethanol solution followed by 12 h of dipping in the dye CH_2Cl_2 solution. Electrochemical impedance measurement data implies that the electron lifetime can be increased by coadsorption of CDCA, which leads to a lower rate of charge recombination and thus improved V_{oc}.

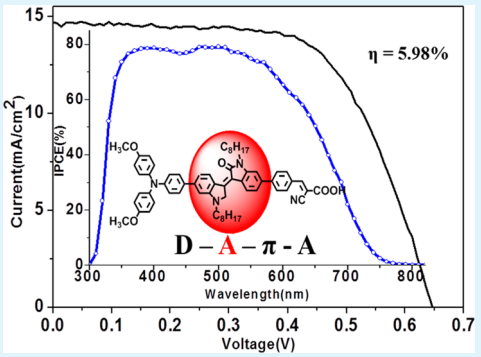

KEYWORDS: *isoindigo, D-A-π-A, broad absorption, chenodeoxycholic acid, solar cells, triarylamine*

INTRODUCTION

Increasing energy demands and concerns over global warming promote the development of renewable energy sources in recent years.[1] Dye-sensitized solar cells (DSSCs) have received close attention in both academia and industry in recent years as cost-effective alternatives to conventional inorganic solar cells.[2] DSSCs based on Ru-complex dyes have been reported with a high conversion efficiency (η) of almost 12.0% under standard AM 1.5 solar light irradiation.[3] However, the rarity and high cost of the ruthenium metal may limit their development for large-scale applications.[4] Recently, a number of new Ru-free sensitizers, such as porphyrin,[5] perylene,[6] cyanine,[7] phenoxazine,[8] suqaraine,[9] coumarin,[10] hemicyaine,[11] indoline,[12] diketopyrrolopyrrole,[13] and bithiazole[14] have been investigated and applied in DSSCs successfully. Nowadays, a D-A-π-A configuration for organic dyes was reported and received increasing attention with an electron withdrawing moiety chromophore incorporated into the common D-π-A structure by inserting the subordinate acceptor, which acts as an electron trap to separate charge and facilitate electron migration to the final acceptor, the sensitizer exhibits broad responsive spectra.[15−17] A high efficiency of nearly 9% under AM 1.5 G irradiation has been achieved on the basis of this type of sensitizers in DSSCs.

Isoindigo has strong electron-withdrawing character because of its two lactam rings. It has been used in the dye industry and biomedicine and can be obtained easily from various natural sources.[18] The perfect palnar π-conjugated structure and the strong-withdrawing effect make it ideal monomer for synthesis of donor/acceptor low band gap conjugated polymer for organic solar cell applications. Hence, applications of isoindigo fall into the scope of renewable and sustainable synthetic sources. Isoindigo-based oligomers were first investigated by Reynolds and co-workers[19] and showed promising absorption spectra and favorable electrochemical and photovoltaic (PV) properties. Recently, the photovoltaic performance of isoindigo-based polymers were independently reported by Zhang et al.,[20] Liu et al.,[21] and Andersson et al.,[22,23] in which the best power conversion efficiency of polymer solar cells was 6.3%. As the isoindigo-based polymers have promising absorption spectra, we consider that the isoindigo can be applied in DSSCs as dye-sensitizers. On the other hand, triarylamine is a well-known nonplanar compound which can improve the hole transporting ability of the materials and prevent the formation of dye aggregates. Also, triphenylamine-based dyes have been widely used in organic photovoltaic functional materials and become the focus of intensive research in the field of solar cells.[24] The introduction of methoxy group to the triphenylamine can expand the extent of electron delocalization over the whole molecule and enhance the ability to donate the electrons of the dyes. In addition, the introduction of the thiophene, furan, and benzene moiety was expected to allow red-shift of

Received: May 23, 2012
Accepted: July 20, 2012
Published: July 20, 2012

 © 2012 American Chemical Society dx.doi.org/10.1021/am300925e | *ACS Appl. Mater. Interfaces* 2012, 4, 4215−4224

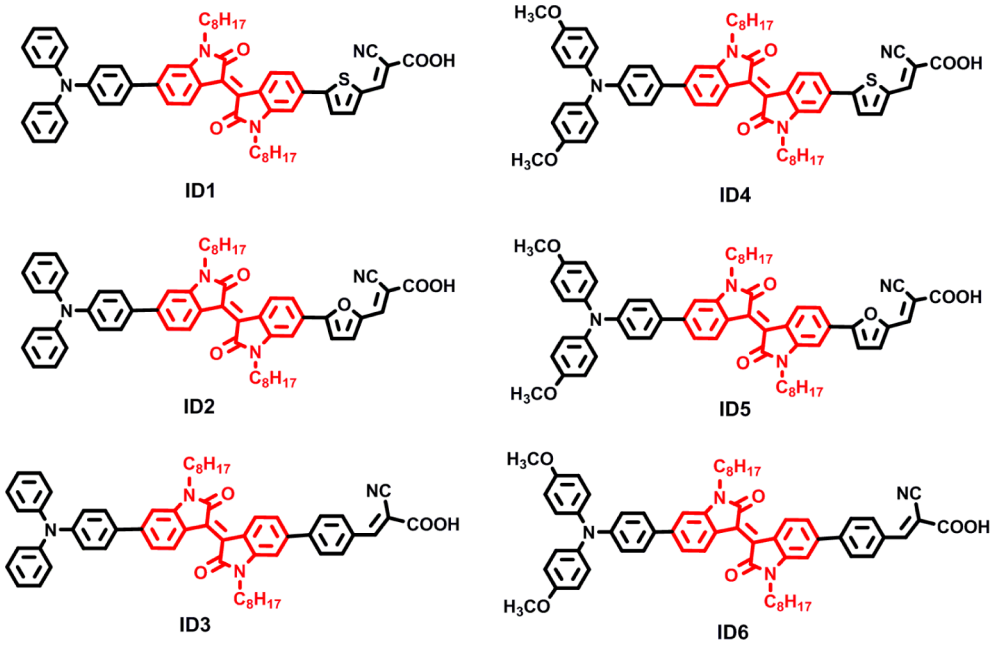

Figure 1. Molecular structures of isoindigo dyes (**ID1**−**ID6**).

the spectrum, and broaden the spectral region of absorption. However, to the best of our knowledge, the dye-sensitizers based on isoindigo for DSSCs have not been reported. Considering these, we have first designed and synthesized six new D-A-π-A organic sensitizers (**ID1**−**ID6** shown in Figure 1), in which triarylamine as the donor, isoindigo as a auxiliary electron withdrawing unit chromophore, thiophene, furan and benzene as the linker, and a cyanoacrylic acid moiety acting as the anchoring group. Finally, the six novel isoindigo-based sensitizers have been successfully applied in the DSSCs and the corresponding photophysical, electrochemical, and photovoltaic properties are also presented.

EXPERIMENTAL SECTION

Materials. Transparent conducting oxide (TCO, 15 Ω /square, F-doped SnO_2, Geao Science and Educational Co. Ltd.) was used as the substrate for the TiO_2 thin-film electrode after several washing. Methoxypropionitrile (MPN) was purchased from Aldrich. Tetra-n-butylammoniumhexafluorophosphate ($TBAPF_6$) and lithium iodide were bought from Fluka and iodine (99.999%) was purchased from Alfa Aesar. Tetrahydrofuran (THF) was predried over 4 Å molecularsieves and distilled under an argon atmosphere from sodium benzophenoneketyl immediately prior to use. *N*,*N*-Dimethyl formamide (DMF) were heated under reflux with calcium hydride and distilled before used. The starting materials 6, 6′-dibromoisoindigo (**1**), and 4-(bis(4-methoxyphenyl)-amino)phenylboronic acid were prepared according to published procedures.[19,25] All other solvents and chemicals used in this work were of reagent grade and used without further purification.

Characterization. ^{1}H NMR and ^{13}C NMR spectra were obtained with a Brücker AM 400 spectrometer. Mass spectra were measured with an HP 5989 mass spectrometer. The UV−vis spectra were measured with a Varian Cary 500 spectrophotometer. Cyclic voltammograms were performed with a Versastat II electrochemical workstation (Princeton applied research) using a normal three-electrode cell with a Pt working electrode, a Pt wire counter electrode, and a regular calomel reference electrode in saturated KCl solution. The electrical impedance spectroscopy (EIS) experiments were performed in the dark by Zahner IM6e Impedance Analyzer, with a frequency range from 0.1 Hz to 100 kHz and a potential modulation of 10 mV. The applied bias potential is held at −0.7 V.

Synthesis of Dyes. *Synthesis of 6,6′-Dibromoisoindigo (1).* 6-Bromooxindole (500 mg, 2.36 mmol) and 6-bromoisatin (533 mg, 2.36 mmol) were dissolved in AcOH (25 mL), followed by the addition of conc. HCl solution (0.1 mL), with the reaction mixture vigorously stirring under reflux for 24 h. After cooling, the mixture was filtered. The solid was washed with water, ethyl alcohol and ethyl acetate. After drying under a vacuum, brown powder was obtained (880 mg, 89%). ^{1}H NMR (400 MHz, $CDCl_3$, ppm): δ: 7.82 (2H, s), 7.69 (2H, d), 7.40 (2H, s), 7.17 (2H, s). ^{13}C NMR (100 MHz, $CDCl_3$, ppm): δ: 170.3, 147.2, 134.0, 132.3, 127.0, 125.3, 122.6, 113.9.

Synthesis of 6,6′-Dibromo-N,N′-(1-octyl)-isoindigo (2). Under nitrogen, compound **1** (420 mg, 1.0 mmol), potassium carbonate (824 mg, 6.0 mmol), and DMF (20 mL) were dissolved in a 50 mL three-necked flask, the mixture was stirred for half an hour, 1-bromooctane (424 mg, 2.2 mmol) was added by a syringe, and then this mixture was heated to 100 °C for 18 h. After cooling, the mixture was poured into water and extracted with CH_2Cl_2. The combined organic layers were washed with brine and water and dried with anhydrous $MgSO_4$, then removed by evaporation, and the residue was purified by column chromatography using silica gel (CH_2Cl_2/petroleum ether) = 1/2 (v/v) as eluent, red powder was obtained (560 mg, 87%). ^{1}H NMR ($CDCl_3$, 400 MHz, ppm): δ: 9.08 (d, J = 8.8 Hz, 2H), 7.17 (dd, J_1 = 1.6 Hz, J_2 = 2.0 Hz, 2H), 6.93 (d, J = 1.6 Hz, 2H), 3.73 (m, 4H), 1.68 (t, 4H), 1.40−1.15 (m, 20H), 0.87(t, 6H).

Synthesis of 4-(6′-Bromo-N,N′-(1-octyl)-isoindigo)-N,N′-bisphenyl aniline (3a). Compound **2** (322 mg, 0.5 mmol), $Pd_2(dba)_3$ (15 mg), P(o-tyl)$_3$ (10 mg) and K_3PO_4 (1.02 g, 5 mmol) in 15 mL of THF were heated to 40−50 °C under a nitrogen atmosphere for 30 min. A solution of 4-(bisphenylamino)phenylbronic acid (145 mg, 0.5 mmol) in THF (10 mL) was transferred to the mixture through a septum. The mixture was then heated to 80 °C and stirred for 12 h. After cooling, the resulting solution was extracted with CH_2Cl_2 (3 × 10 mL). The organic portion was combined and washed with brine and water and dried with anhydrous $MgSO_4$. The solvent was removed by evaporation, the residue was purified by column chromatography using silica gel (PE/CH_2Cl_2 = 4/1−2/1, v/v) to give a purple solid (163 mg). Yield: 40.3%. ^{1}H NMR($CDCl_3$, 400 MHz, ppm): δ 9.20 (d, J = 8 Hz, 1H), 9.08 (d, J = 8 Hz, 1H),7.52 (d, J = 8 Hz, 2H), 7.31−7.27 (m,4H), 7.24 (dd, J_1 = 8 Hz, J_2 = 8 Hz, 1H), 7.18−7.13 (m, 7H), 7.09−7.05 (m, 2H), 6.94 (dd, J_1= 8 Hz, J_2= 8 Hz, 2H), 3.82−3.73 (m, 4H), 1.73−1.69 (m, 4H), 1.38−1.25 (m, 20H), 0.89−0.83 (m, 6H).

Synthesis of 4-(6′-Bromo-N,N′-(1-octyl)-isoindigo)-N,N′-bis(4-methoxy phenyl)) Aniline (3b). **3b** was obtained as purple solid in similar

way to **3a**. Yield: 50.7%. ^{1}H NMR($CDCl_3$, 400 MHz, ppm): δ 9.18 (d, J = 8 Hz, 1H), 9.07 (d, J = 8 Hz, 1H), 7.47 (d, J = 8 Hz, 2H), 7.22 (dd, J_1 = 4 Hz, J_2 = 4 Hz,1H), 7.16 (dd, J_1 = 4 Hz, J_2 = 4 Hz,1H), 7.12−7.09 (m, 4H), 7.00 (s, 1H), 6.97 (s, 1H), 6.93 (d, J = 4 Hz, 2H), 6.88−6.84 (m, 4H), 3.79−3.63 (m, 4H), 1.73−1.65 (m, 4H), 1.37−1.22 (m, 20H), 0.89−0.83 (m, 6H).

*Synthesis of 6-(6′-(4-(Diphenylamino)phenyl)-N,N′-(1-octyl)-isoindigo)-thiophene-2-carbaldehyde (**4ac**).* Compound **3a** (162 mg, 0.2 mmol), $Pd_2(dba)_3$ (15 mg), P(o-tyl)$_3$ (10 mg), and K_3PO_4 (1.02 g, 5 mmol) in 15 mL of THF were heated to 40−50 °C for 30 min. A solution of 5-formylthiophen-2-yl boronic acid (100 mg, 0.6 mmol) in THF (5 mL) was transferred to the mixture through a septum. The mixture was then heated up to 80 °C and stirred for 12 h. After cooling, the resulting solution was extracted with CH_2Cl_2 (3 × 10 mL). The organic portion was combined and washed with brine and water and dried with anhydrous $MgSO_4$. The solvent was removed by evaporation, the residue was purified by column chromatography using silica gel (PE/CH_2Cl_2 = 2/1−1/1, v/v) to give a purple solid (134 mg). Yield: 80.2%. ^{1}H NMR($CDCl_3$, 400 MHz, ppm): δ 9.91 (s, 1H), 9.24 (d, J = 8 Hz, 1H), 9.21 (d, J = 8 Hz, 1H),7.76 (d, J = 4 Hz, 1H), 7.53 (d, J = 8 Hz, 2H), 7.50 (d, J = 4 Hz, 1H), 7.36 (dd, J_1 = 8 Hz, J_2 = 8 Hz, 2H), 7.29 (m, 4H), 7.25 (d, J = 4 Hz, 1H), 7.16 (m, 6H), 7.06 (m, 3H), 7.02 (s, 1H), 6.95 (s, 1H), 3.83 (m, 4H), 1.76−1.72 (m, 4H), 1.32−1.25 (m, 20H), 0.88−0.84 (m, 6H).

*Synthesis of 6-(6′-(4-(Diphenylamino)phenyl)-N,N′-(1-octyl)-isoindigo)-furan-2-carbaldehyde (**4ad**).* **4ad** was obtained as purple solid in similar way to **4ac**. Yield: 76.2%.^{1}H NMR ($CDCl_3$, 400 MHz, ppm): δ 9.70 (s, 1H), 9.26 (d, J = 12 Hz, 1H), 9.21 (d, J = 8 Hz, 1H), 7.54 (d, J = 8 Hz, 2H), 7.45 (dd, J_1 = 12 Hz, J_2 = 8 Hz, 1H), 7.37 (d, J = 4 Hz, 1H), 7.32−7.24 (m, 6H), 7.17−7.13 (m, 6H), 7.07 (t, 2H), 6.97 (s, 1H), 6.96 (s, 1H), 3.84−3.82 (m, 4H), 1.75−1.72 (m, 4H), 1.42−1.25 (m, 20H), 0.88−0.84 (m, 6H).

*Synthesis of 6-(6′-(4-(Diphenylamino)phenyl)-N,N′-(1-octyl)-isoindigo)- benaldehyde (**4ae**).* **4ae** was obtained as purple solid in similar way to **4ac**. Yield: 86.1%. ^{1}H NMR ($CDCl_3$, 400 MHz, ppm): δ 10.08 (s, 1H), 9.29 (d, J = 8 Hz, 1H), 9.24 (d, J = 8 Hz, 1H), 7.99 (d, J = 8 Hz, 2H), 7.81 (d, J = 8 Hz, 2H), 7.53 (d, J = 8 Hz, 2H), 7.33−7.25 (m, 6H), 7.17−7.14 (m, 6H), 7.07 (m, 2H), 7.01 (s, 1H), 6.97 (s, 1H), 3.85−3.81 (m, 4H), 1.76−1.75 (m, 4H), 1.42−1.26 (m, 20H), 0.87−0.84 (m, 6H).

*Synthesis of 6-(6′-(4-(Bis(4-methoxyphenyl)amino) phenyl)-N,N′-(1-octy-l)-isoindigo)-thiophene-2-carbaldehyde (**4bc**).* **4bc** was obtained as purple solid in similar way to **4ac**. Yield: 88.2%. ^{1}H NMR ($CDCl_3$, 400 MHz, ppm): δ 9.92 (s, 1H), 9.24 (d, J = 8 Hz, 1H), 9.19 (d, J = 8 Hz, 1H), 7.77 (d, J = 4 Hz, 1H), 7.50−7.47 (m, 3H), 7.36 (dd, J_1 = 8 Hz, J_2 = 8 Hz, 1H), 7.23 (dd, J_1 = 8 Hz, J_2 = 8 Hz, 1H), 7.11 (d, J = 8 Hz, 4H), 7.03 (d, J = 4 Hz, 1H), 6.99 (d, J = 8 Hz, 2H), 6.94 (s, 1H), 6.89−6.85 (m, 4H), 3.86−3.79 (m, 4H), 1.73 (m, 4H), 1.42−1.26 (m, 20H), 0.88−0.84 (m, 6H).

*Synthesis of 6-(6′-(4-(Bis(4-methoxyphenyl)amino) phenyl)-N,N′-(1-octy-l)-isoindigo)-furan-2-carbaldehyde (**4bd**).* **4bd** was obtained as purple solid in similar way to **4ac**. Yield: 88.2%. ^{1}H NMR($CDCl_3$, 400 MHz, ppm): δ 9.70 (s, 1H), 9.25 (d, J = 8 Hz, 1H), 9.19 (d, J = 8 Hz, 1H), 7.48 (d, J = 8 Hz, 2H), 7.44 (d, J = 8 Hz, 1H), 7.36 (d, J = 4 Hz, 1H), 7.24−7.22 (m, 2H), 7.13−7.09 (m, 4H), 6.99 (d, J = 8 Hz, 2H), 6.95 (d, J = 4 Hz, 1H), 6.93 (s, 1H), 6.88−6.85 (m, 4H), 3.88−3.79 (m, 10H), 1.77−1.71 (m, 4H), 1.43−1.26 (m, 20H), 0.88−0.84 (m, 6H).

*Synthesis of 6-(6′-(4-(Bis(4-methoxyphenyl)amino)phenyl)-N,N′-(1-oct-yl)-isoindigo)-benaldehyde (**4be**).* **4be** was obtained as purple solid in similar way to **4ac**. Yield: 81.2%. ^{1}H NMR($CDCl_3$, 400 MHz, ppm): δ 10.08 (s, 1H), 9.28 (d, J = 8 Hz, 1H), 9.21 (d, J = 8 Hz, 1H), 7.99 (d, J = 8 Hz, 2H), 7.80 (d, J = 8 Hz, 2H), 7.48 (d, J = 8 Hz, 2H), 7.31(dd, J_1 = 8 Hz, J_2 = 8 Hz, 1H), 7.25 (dd, J_1 = 12 Hz, J_2 = 12 Hz, 1H), 7.13−7.10 (m, 4H), 7.01 (d, J = 4 Hz, 2H), 6.98 (s, 1H), 6.95 (s, 1H), 6.89−6.85 (m, 4H), 3.88−3.81 (m, 4H), 1.77−1.72 (m, 4H), 1.43−1.26 (m, 20H), 0.87−0.84 (m, 6H).

*Synthesis of 2-Cyano-3-(6-(6′-(4-(diphenylamino)phenyl)-N,N′-(1-octyl)-isoindigo)-thiophene-2-yl-)acrylic Acid (**ID1**).* Compound **4ac** (100 mg, 0.12 mmol), 2-cyanoacetic acid (85 mg, 1 mmol), ammonium acetate (120 mg), and acetic acid (8 mL) at 120 °C for 12 h. After cooling, the mixture was poured into water. The precipitate was filtered and washed with water. The residue was purified by column chromatography using silica gel (CH_2Cl_2/ethanol = 10/1, v/v) to yield 88 mg of dark purple solid.Yield: 81%. ^{1}H NMR($CDCl_3$, 400 MHz, ppm): δ 9.09 (t, 2H), 8.15 (s, 1H), 7.85 (d, J = 4 Hz, 1H), 7.76 (d, J = 4 Hz, 1H), 7.34−7.21 (m,6H), 7.13−7.05 (m,6H), 7.00 (d, J = 8 Hz, 2H), 3.81 (m, 4H), 1.64−1.61 (m, 4H), 1.31−1.22 (m, 20H), 0.85−0.78 (m, 6H). ^{13}CNMR(THF-d_8, 100 MHz, ppm): δ 165.8, 165.7, 146.0, 145.6, 143.6, 142.2, 142.0, 141.0, 140.3, 132.0, 131.7, 130.5, 129.2, 129.0, 128.6, 127.4, 125.7, 125.0, 122.8, 121.3, 121.0, 120.0, 118.7, 117.9, 117.3, 115.8, 103.5, 103.1, 37.6, 30.0, 27.8, 27.5, 27.4, 25.7, 25.2, 20.7, 11.7. HRMS (ESI, m/z): [M − H]$^-$ calcd for ($C_{58}H_{57}N_4O_4S$), 905.4101; found, 905.4103.

*Synthesis of 2-Cyano-3-(6-(6′-(4-(diphenylamino)phenyl)-N,N′-(1-octyl)-isoindigo)-furan-2-yl-)acrylic Acid (**ID2**).* A procedure similar to that for the dye **ID1** but with compound **4ad** (123 mg, 0.15 mmol) instead of compound **4ac** giving the dye **ID2** as a dark purple solid (106 mg, yield: 79.4%). ^{1}H NMR(DMSO, 400 MHz, ppm): δ 9.06 (m, 2H), 7.82 (s, 1H), 7.81 (d, J = 8 Hz, 1H), 7.63 (d, J = 8 Hz, 2H), 7.41−7.31 (m,6H), 7.20 (d, J = 4 Hz, 2H), 7.14−7.08 (m,3H), 7.04 (d, J = 8 Hz, 4H), 6.97 (d, J = 8 Hz, 2H), 3.74 (m, 4H), 1.64−1.61 (m, 4H), 1.34−1.22 (m, 20H), 0.85−0.78 (m, 6H). ^{13}CNMR(DMSO, 100 MHz, ppm): δ 167.8, 164.5, 146.8, 145.9, 145.3, 144.6, 142.0, 134.1, 132.6, 131.8, 130.7, 130.5, 129.6, 127.8, 124.5, 123.5, 122.2, 121.0, 117.8, 111.1, 109.2, 105.6, 103.8, 34.1, 31.7, 29.8, 29.0, 28.6, 26.7, 26.0, 22.0, 13.8. HRMS (ESI, m/z): [M − H]$^-$ calcd for ($C_{58}H_{57}N_4O_5$), 889.4329; found, 889.4355.

*Synthesis of 2-Cyano-3-(6-(6′-(4-(diphenylamino)phenyl)-N,N′-(1-octyl)-isoindigo)-phenyl)acrylic Acid (**ID3**).* A procedure similar to that for the dye **ID1** was followed but with compound **4ae** (100 mg, 0.12 mmol) instead of compound **4ac**, giving the dye **ID3** as a dark purple solid (84 mg, yield: 77.8%). ^{1}HNMR(THF-d_8, 400 MHz, ppm): δ 9.18 (s, 2H), 8.27 (s, 1H), 7.88 (s, 2H), 7.61−7.54 (m, 2H), 7.39 (s, 2H), 7.14 (t, 4H), 6.98−6.96 (d, 6H), 6.94−6.84 (m, 6H), 3.73−3.69 (m, 4H), 1.64−1.60 (m, 4H), 1.28−1.24 (m, 20H), 0.78−0.73 (m, 6H). ^{13}CNMR(THF-d_8, 100 MHz, ppm): δ 165.8, 165.7, 146.0, 145.6, 143.7, 143.4, 142.0, 141.0, 140.3, 132.0, 131.7, 130.5, 129.2, 129.0, 128.5, 127.4, 125.7, 125.0, 122.8, 121.3, 121.0, 120.0, 118.7, 117.9, 117.3, 115.8, 103.5, 103.1, 37.6, 30.0, 28.8, 27.8, 27.5, 27.4, 25.7, 25.2, 20.7, 11.7. HRMS (ESI, m/z): [M − H]$^-$ calcd for ($C_{60}H_{59}N_4O_4$), 899.4536; found, 899.4537.

*Synthesis of 2-Cyano-3-(6-(6′-(4-(bis(4-methoxyphenyl)amino)-phenyl)-N,N′-(1-octyl)-isoindigo)-thiophene-2-yl-)acrylic Acid (**ID4**).* A procedure similar to that for the dye **ID1** was followed but with compound **4bc** (90 mg, 0.1 mmol) instead of compound **4ac**, giving the dye **ID4** as a blue green solid (80 mg, yield: 82.7%). ^{1}H NMR($CDCl_3$, 400 MHz, ppm): δ 9.05 (d, J = 8 Hz,1H), 9.02 (d, J = 8 Hz,1H), 8.10 (s, 1H), 7.78 (s, 1H), 7.71(s, 1H), 7.52 (d, J = 12 Hz,2H), 7.22−7.19 (m,2H), 7.13 (d, J = 8 Hz, 1H), 7.09 (s, 1H), 7.03 (d, J = 8 Hz, 4H), 6.92 (d, J = 8 Hz, 4H), 6.79 (d, J = 8 Hz, 2H), 3.75−3.72 (m, 4H), 1.61(m, 4H), 1.35−1.22 (m, 20H), 0.86−0.78 (m, 6H). ^{13}CNMR(DMSO, 100 MHz, ppm): δ 167.2, 167.1, 163.8, 162.26, 156.0, 148.2, 145.0, 144.5, 143.8, 139.5, 137.0, 136.1, 135.5, 131.9, 130.2, 130.0, 129.8, 127.4, 126.9, 125.7, 121.3, 119.2, 118.6, 114.9, 104.9, 104.4, 55.2, 31.2, 31.1, 29.0, 26.8, 22.0, 13.8. HRMS (ESI, m/z): [M + H]$^+$ calcd for ($C_{60}H_{63}N_4O_6S$), 967.4468; found, 967.4465.

*Synthesis of 2-Cyano-3-(6-(6′-(4-(bis(4-methoxyphenyl)amino)-phenyl)-N,N′-(1-octyl)-isoindigo)-furan-2-yl-)acrylic Acid (**ID5**).* A procedure similar to that for the dye **ID1** was followed but with compound **4bd** (110 mg, 0.12 mmol) instead of compound **4ac**, giving the dye **ID5** as a blue green solid (100 mg, yield: 85.1%). ^{1}H NMR(DMSO, 400 MHz, ppm): δ 9.06 (d, J = 8 Hz,1H), 9.00 (d, J = 8 Hz, 1H), 7.79 (s, 1H), 7.52 (d, J = 8 Hz, 2H), 7.38 (d, J = 8 Hz, 1H), 7.33−7.31 (m, 2H), 7.18 (d, J = 4 Hz, 1H), 7.13 (d, J = 8 Hz, 1H), 7.06−7.01 (m, 5H), 6.92 (d, J = 8 Hz, 4H), 6.78 (d, J = 8 Hz, 2H), 3.75−3.72 (m, 4H), 1.60 (m, 4H), 1.30−1.21 (m, 20H), 0.85−0.78 (m, 6H). ^{13}CNMR (DMSO, 100 MHz, ppm): δ 167.7, 167.0, 162.5, 155.6, 155.1, 142.8, 141.1, 139.5, 134.4, 131.6, 131.3, 130.3, 129.4, 127.7, 127.0, 126.0, 125.5, 124.1, 119.2, 115.0, 113.0, 111.0, 108.0,

Scheme 1. Synthetic Routes of the Six Isoindigo Dyes (ID1−ID6)[a]

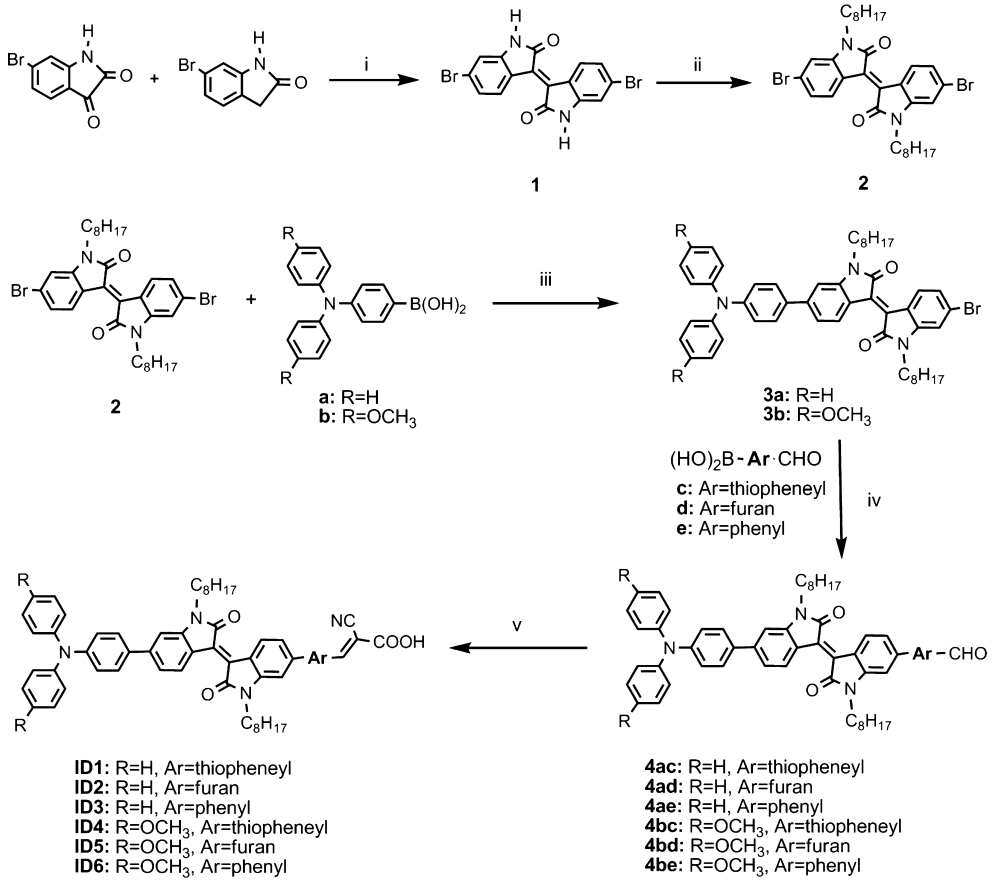

[a](i) AcOH, conc. HCl solution, reflux for 24h; (ii) DMF, K_2CO_3, 1-bromooctane, 100 °C for 18h; (iii) $Pd_2(dba)_3$, P(o-tyl)$_3$, K_3PO_4, THF, 80 °C for 20h; (iv) $Pd_2(dba)_3$, P(o-tyl)$_3$, K_3PO_4, THF, 80 °C for 20h; (v) CH_3COOH, CH_3COONH_4, 120 °C for 10h.

104.1, 97.8, 74.6, 72.7, 69.8, 55.2, 36.1, 35.1, 33.3, 31.2, 30.3, 29.0, 27.0, 24.7, 22.0, 17.3, 13.9. HRMS (ESI, *m/z*): [M − H]$^-$ calcd for ($C_{60}H_{62}N_4O_7$), 949.4540; found, 949.4547.

*Synthesis of 2-Cyano-3-(6-(6′-(4-(bis(4-methoxyphenyl)amino)-phenyl)-N,N′-(1-octyl)-isoindigo)-phenyl)acrylic Acid (**ID6**).* A procedure similar to that for the dye **ID1** but with compound **4be** (116 mg, 0.13 mmol) instead of compound **4ac** giving the dye **ID6** as a blue green solid (90 mg, yield: 72.1%). ^{1}H NMR(DMSO, 400 MHz, ppm): δ 9.13 (m, 2H), 8.03 (s, 1H), 7.97−7.93 (m, 4H), 7.60 (s, 2H), 7.38 (s,2H), 7.20 (s, 2H), 7.07 (d, *J* = 8 Hz, 4H), 6.94 (d, *J* = 8 Hz, 4H), 6.82 (d, *J* = 8 Hz, 2H) 3.82−3.76 (m, 4H), 1.65 (m, 4H), 1.32−1.23 (m, 20H), 0.85−0.81 (m, 6H).^{13}CNMR(DMSO, 100 MHz, ppm): δ 167.3, 167.2, 163.6, 156.0, 148.6, 147.8, 145.1, 144.7, 143.8, 141.9, 141.3, 139.6, 132.6, 132.0, 130.3, 130.0, 129.6, 129.1, 127.5, 127.0, 120.9, 119.8, 119.2, 118.7, 114.9, 105.9, 105.0, 55.2, 31.2, 28.6, 27.0, 26.3, 22.0, 13.9.HRMS (ESI, *m/z*): [M − H]$^-$ calcd for ($C_{62}H_{63}N_4O_6$), 959.4748; found, 959.4742.

Device Fabrication. A layer of ca. 5 μm TiO_2 (13 nm paste, T/SP) was coated on the FTO conducting glass by screen printing and then dried for 6 min at 125 °C. This procedure was repeated 2 times (ca. 10 μm) and finally coated by a layer (ca. 4 μm) of TiO_2 paste (Ti-nanoxide 300) as the scattering layer. The trilayer TiO_2 electrodes were gradually heated under an air flow at 275 °C for 5 min, 325 °C for5 min, 375 °C for 5 min, 450 °C for 15 min, and 500 °C for 15 min. The sintered film was further treated with 0.04 M $TiCl_4$ aqueous solution at room temperature for 12 h, after being washed with deionized water and fully rinsed with ethanol, the films were heated again at 450 °C followed by cooling to 50 °C and dipping into a 5 × 10^{-4} M dye bath in CH_2Cl_2 solution and maintained overnight for 12 h at room temperature. To scrutinize and optimize the concentration of CDCA, TiO_2 films were immersed in CDCA ethanol solution for 6 h before dipping into dye CH_2Cl_2 solution. The electrode was then rinsed with toluene and dried. The size of the TiO_2 electrodes used was 0.25 cm^2. The dye adsorbed TiO_2 photoanodes and Pt counter electrode were sealed together by heating with a 25 μm hot-melt (Surlyn 1702, Dupont) as a spacer to produce a sandwich-type cell. The electrolyte consisting of 0.05 M I_2, 0.5 M LiI in a mixture of acetonitrile and methoxypropionitrile (7:3, v/v) was injected through a hole in the back of the counter electrode. Finally, the hole was sealed using a UV-meltgum and a cover glass.

Photovoltaic Property Measurements. The DSSCs were evaluated by recording the *J*−*V* curves with a Keithley 2400 digital source meter under the illumination of AM 1.5 solar simulator equipped with a 300 W xenon lamp (Model No. 91160, Oriel). The power of the simulated light was calibrated to 100 mW cm^{-2} using a Newport Oriel PV reference cell system (model 91150 V). The voltage step and delay time of photocurrent were 10 mV and 40 ms, respectively. Cell active area was tested with a mask of 0.25 cm^2. Incident monochromatic photon-to-electron conversion efficiency (IPCE) spectra were obtained with an Newport-74125 system (Newport Instruments). The intensity of monochromatic light was measured with a Si detector (Newport-71640).

RESULTS AND DISCUSSION

Synthesis. Scheme 1 outlines the synthesis of the six isoindigo-based dyes (**ID1−ID6**). 6, 6′-Dibromoisoindigo was easily synthesized in high yield by refluxing the commercially available 6-bromoisatin and 6-bromooxindole in a mixture of acetic acid and hydrochloric acid. To improve the solubility of isoindigo monomer, the octyl chain was attached to both lactam nitrogen atoms. Also, the alkyl chains can help to form a

blocking layer to keep I_3^- ions away from the TiO_2 electrode surface, hence increasing the electron lifetime and open circuit voltage (V_{oc}).[26] 4-Triphenylamine and 4-methoxy-*N*-(4-methoxyphenyl)-*N*-phenylbenzenamine group as donor are attached to the core isoindigo by Suzuki coupling reaction. The reaction produced the disubstituted side products, fortunately monocapped compounds can be easily separated by column chromatography. In the next step, these two bromo-exposed intermediates reacted with 5-formylthiophen-2-ylboronic acid, 5-formylfuran-2-yl-boronic acid, or 4-formylphenylboronic acid by Suzuki coupling reaction, respectively. The corresponding carbaldehydes were finally converted to the target dyes (**ID1**−**ID6**) via Knoevenagel condensation. All the key intermediates and six novel organic isoindigo sensitizers (**ID1**−**ID6**) were confirmed by ^{1}H NMR, ^{13}C NMR, and HRMS in the Experimental Section.

Photophysical Properties. Absorption spectra of the six dyes (**ID1-ID6**) in CH_2Cl_2 are shown in Figure 2 and the corresponding data are summarized in Table 1. In the UV−vis spectra in Figure 2, these dyes exhibit two major prominent bands, appearing at 396−431 and 537−589 nm, respectively. The former may be attributed to a localized aromatic $\pi-\pi^*$ transition of isoindigo with thiophene, furan, or benezene unit and cynaoacrylic acid part. The origination of the absorption band will be further discussed by the following theoretical simulation. The absorption at around 537−589 nm can be ascribed to the intramolecular charge transfer (ICT) between the triarylamine donor part and the cyanoacetic acceptor moiety, in which the absorption maximum of **ID1**−**ID6** are at 563, 571, 537, 584, 589, and 568 nm, respectively. For three dyes (**ID1**−**ID3**) with triphenylamine unit as electron donor, **ID1** and **ID2** have similar absorption properties. Compared with **ID1** and **ID2**, **ID3** exhibits about 26 nm blue-shifted absorption. Meanwhile, the similar phenomena are observed for the other three dyes (**ID4**−**ID6**), in which **ID6** exhibits about 16 and 21 nm blue-shifted absorption than **ID4** and **ID5**, respectively. It could be explained that the decline in coplanarity between isoindigo unit and the anchoring part due to the introduction of benzene moiety. Also, the dihedral angles formed between the isoindigo rings and π-spacer near anchoring moiety in **ID1**−**ID6** are computed to be 22.5, 1.7, 34.3, 22.9, 1.6, and 34.2°, respectively (Figure 4). The relative large dihedral angles for isoindigo and benzene-bridged **ID3** and **ID6** further explained the reason of large blue-shift absorption in solution. In addition, the donor effect on absorption peak is also distinct. The bathochromic shift by 21, 18, or 31 nm is observed when replacing triphenylamine unit (**ID1**−**ID3**) with 4-methoxy-*N*-(4-methoxyphenyl)-*N*-phenylbenze namine unit (**ID4**−**ID6**) in the donor moiety. The introduction of two methoxy groups on the triphenylamine on the electron donor side can increase the extent of electron delocalization over the whole molecule and the ability to electron donor of the dyes, thus the maximum absorption peaks of **ID4**−**ID6** are red-shifted a little bit. Consequently, the isoindigo-based sensitizers can result in broader spectral range near NIR region and beneficial to light-harvesting for higher electricity conversion efficiency.

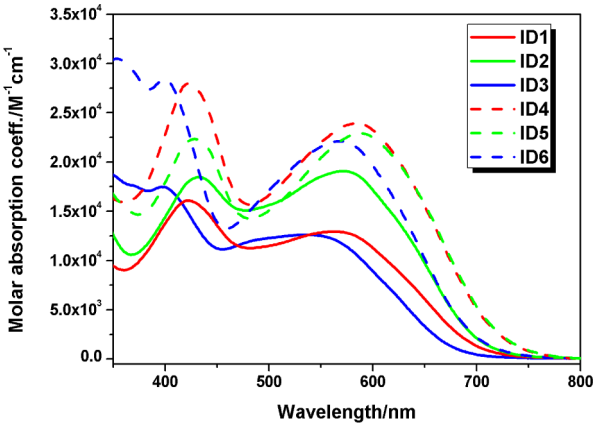

Figure 2. Absorption spectra of **ID1**−**ID6** in CH_2Cl_2.

Table 1. Optical and Electrochemical Properties of Isoindigo Dyes (ID1−ID6)

Dye	λ_{max}[a] (nm) (ε ($\times 10^{-4}$ $M^{-1}cm^{-1}$))	λ_{max}[b] (nm)	HOMO[c] (V) (vs NHE)	E_{0-0}[d] (eV)	LUMO[e] (V) (vs NHE)
ID1	420 (1.50) 563 (1.30)	542	1.03	1.71	−0.68
ID2	431 (1.80) 571 (1.90)	548	1.05	1.68	−0.63
ID3	396 (1.79) 537 (1.26)	517	1.03	1.76	−0.73
ID4	423 (2.80) 584 (2.39)	555	0.81	1.63	−0.82
ID5	429 (2.20) 589 (2.29)	560	0.79	1.60	−0.81
ID6	399 (2.82) 568 (2.21)	540	0.79	1.65	−0.86

[a]Absorption maximum in CH_2Cl_2 solution (3×10^{-5} M). [b]Absorption maximum on TiO_2 film (without CDCA). [c]HOMO were internally calibrated with ferrocene (0.4 V versua NHE) in CH_2Cl_2. [d]E_{0-0} was derived from the wavelength at absorption thresholds from absorption spectra for the dyes-loaded 2 μm TiO_2 films. [e]LUMO is calculated by subtracting E_{0-0} to HOMO.

The absorption spectra of **ID1**−**ID6** on 2 μm TiO_2 films are shown in Figure 3. The maximum absorption peaks for **ID1**−**ID6** on the TiO_2 film are at 542, 548, 517, 555, 560, and 540 nm, respectively. Compared with the solution absorption, the absorption bands of the dyes on the TiO_2 films are blue-shifted by 21, 23, 20, 29, 29, and 28 nm, respectively. Generally, the sensitizers have a tendency to aggregate at solid−liquid interface when they are adsorbed onto the TiO_2 films. The experimental results in this work indicate that **ID1**−**ID6** form blue-shifted H-aggregates on the TiO_2 surface. In addition, after the dyes adsorb on TiO_2 film, the weaker electron-withdrawing

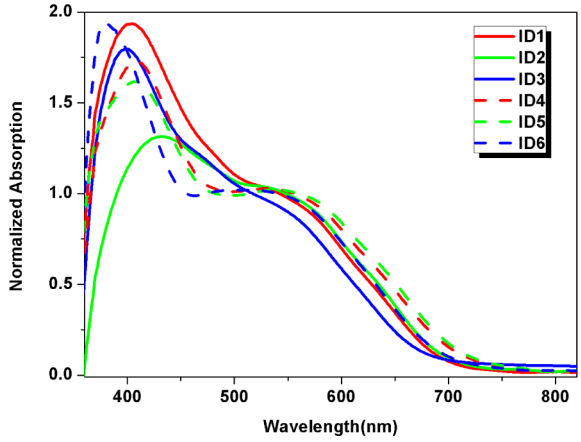

Figure 3. Normalized absorption spectra of **ID1**−**ID6** on 2 μm transparent TiO_2 films.

dx.doi.org/10.1021/am300925e | ACS Appl. Mater. Interfaces 2012, 4, 4215−4224

ability of the acceptor (carboxylate-TiO_2 unit) compared to the carboxylic acid can also cause the blue-shifted absorption peak.[27] Therefore, the blue shifts of the absorption spectra of **ID1−ID6** on TiO_2 film are caused by the H-aggregates and deprotonation of the carboxylic acid.

Electrochemical Properties. To evaluate the possibility of electron injection and dye regeneration on the conduction band of TiO_2, cyclic voltammetry were performed in THF solution with ferrocene/ferrocenium (Fc/Fc^+) redox couple as an external standard. The highest occupied molecular orbitals (HOMOs) of **ID1−ID6** corresponding to their first redox potential are 1.03, 1.05, 1.03, 0.81, 0.79, and 0.79 V versus NHE, respectively. It is clear that the HOMO levels of **ID4−ID6** are higher than those of **ID1−ID3**, which is in agreement with the order of the increase of electron-donating ability of the donors: 4-(Bis(4-methoxyphenyl)amino)phenyl >4-(diphenylamino)phenyl. Generally, the stronger electron-donating ability of the donor resulted in a higher HOMO energy level. The band gap energies ($E_{(0-0)}$) of the six dyes (**ID1−ID6**) were 1.71, 1.68, 1.76, 1.63, 1.60, and 1.65 eV, respectively, which were calculated from their absorption thresholds of dye adsorbed TiO_2 films. The estimated excited state potential corresponding to the lowest unoccupied molecular orbital (LUMO) levels, calculated from $E_{HOMO} - E_{0-0}$, are −0.68, −0.63, −0.73, −0.82, −0.81, and −0.86 V versus NHE, respectively. The HOMO and LUMO levels of the six dyes were collected in Table 1. Consequently, we found the LUMO levels of **ID1−ID6** were more negative than the conduction band (E_{cb}) of the TiO_2 electrode (−0.5 V versus NHE), indicating that electron injection from the LUMO orbital into the conduction band of TiO_2 is energetically permitted.[28] The HOMO levels of **ID1−ID6** to be sufficiently more positive than the I^-/I_3^- redox couple (0.4 V), ensuring the thermodynamic regeneration of dyes.

Theoretical Approach. Density functional theory (DFT) and time-dependent density functional theory (TDDFT) calculations were carried out with the Gaussian 09 package[29] to further investigate the electron distribution for the frontier molecular orbitals and the electronic transition processes upon photoexcitation. The ground-state geometries of dyes **ID1−ID6** have been optimized in the gas phase by DFT by using the hybrid B3LYP[30] functional and the standard 6-31G(d) basis set. For the TDDFT calculations, performed on the B3LYP-optimized ground-state geometries, the Coulomb attenuating B3LYP (CAM-B3LYP) approach[31] was used with 6-31+G(d) basis set. Solvation effect was taken into account into the TDDFT calculations in CH_2Cl_2 with the nonequilibrium version of the C-PCM model[32] implemented in Gaussian09.[29] The TDDFT results and frontier molecular orbitals of **ID1−ID6** are shown in Table 2 and Figure 4, respectively.

The electronic transitions shown by the TDDFT calculation indicate that the absorption bands of **ID1−ID6** with λ_{max} at 533.4−583.9 and 373.5−400.7 nm are ascribed to HOMO → LUMO and HOMO-3 → LUMO transitions, respectively (Table 2). The six calculated lowest electronic transitions for **ID1-ID6** are consistent with the experimental data (Table 1). The HOMO orbitals of **ID1−ID6** are a π orbital mainly located on triphenylamine or 4-(bis(4-methoxyphenyl)amino)phenyl donor part, whereas their HOMO-3 orbitals are a π orbital distributed on the isoindigo core part, aromatic rings and cyanoacrylic acid unit except for **ID6** (Figure 4). The electron distributions of LUMOs are delocalized over the aromatic rings, thiophene, furan and benzene moiety and cyanoacetic acid part.

Table 2. Calculated TDDFT Excitation Energies (nm), Oscillator Strengths (f), and Composition in Terms of Molecular Orbital Contributions of ID1−ID6

compds	state	composition[a]	E (nm)	f
ID1	S1	63% H→L	556.9	1.3918
	S2	53% H-3→L	396.3	0.7405
ID2	S1	62% H→L	562.3	1.3034
	S2	64% H-3→L	399.5	0.6416
ID3	S1	62% H→L	533.4	1.243
	S2	60% H-3→L	373.5	0.9869
ID4	S1	81% H→L	579.9	1.3597
	S2	42% H-3→L	387.4	0.4968
ID5	S1	68% H→L	583.9	1.3081
	S2	55% H-3→L	400.7	0.6065
ID6	S1	69% H→L	555.2	1.2505
	S2	62% H-3→L	374.7	1.0133

[a]H = HOMO, L = LUMO, H-3 = HOMO-3.

The electron dominated by anchoring group also suggests that the excitation from the HOMO to the LUMO orbital can move the electron distribution from the triarylamine donor unit to the cyanoacrylic acid anchoring group to realize electron injection to the conduction band of TiO_2. Apparently, the observed absorption bands at λ_{max} = 396−431 nm are favorable to the photon-to-electron conversion because they correspond to the efficient electron transitions from HOMO-3 to the LUMO orbital.

Photovoltaic Performance of DSSCs. Figure 5 shows the incident photon-to-current conversion efficiency (IPCE) as function of incident wavelength for DSSCs based on **ID1−ID6**. Generally, the solar cells sensitized by **ID4−ID6** have better performances than **ID1−ID3** at the range of 350−650 nm, especially for **ID1** and **ID3** at the range of 380−700 nm. The IPCE of **ID6** exceeds 75.0% in the spectral range of 400−550 nm, which reaches its maximum value of 79.0% at 470 nm. The **ID2**-, **ID4**- and **ID5**-sensitized cells output the IPCE values above 60.0% at the range of 350−600 nm, whereas the IPCE values of **ID1** and **ID3** reduce significantly above 550 nm. This leads to the poor performance for the **ID1** and **ID3** based DSSCs at the photoelectron efficiency. The thresholds wavelength of the IPCE spectra for all the dyes were located at below 800 nm, especially for **ID3** at about 750 nm, which is consistent with the threshold wavelength of absorption spectra when adsorbed onto TiO_2 films.

Figure 6 presents the current−voltage characteristics of DSSCs fabricated with these isoindigo dyes (**ID1−ID6**) as sensitizers under standard global AM 1.5 solar light conditions. The detailed parameters of short-circuit current density (J_{sc}), open-circuit voltage (V_{oc}), fill factor (ff), and photovoltaic conversion efficiency (η) are collected in Table 3. In general, the photocurrent of the dyes **ID4−ID6** with 4-(bis(4-methoxyphenyl)amino)phenyl as electron donor was higher than the other dyes **ID1−ID3** containing triphenylamine as donor. This may be caused by the higher molar extinction coefficient of **ID4−ID6**, which yields better light harvesting and higher short circuit current; on the other hand, the much more negative LUMO levels of **ID4−ID6** lead to more efficient electron injection from excited state dyes to the conduct band of TiO_2 film because the incorporation of methoxy groups to the triphenylamine enhance the extent of electron delocalization. Consistent with the results of IPCE, the J_{sc} of these six dyes decrease with the order of **ID6**, **ID4**, **ID5**, **ID2**, **ID1**, and

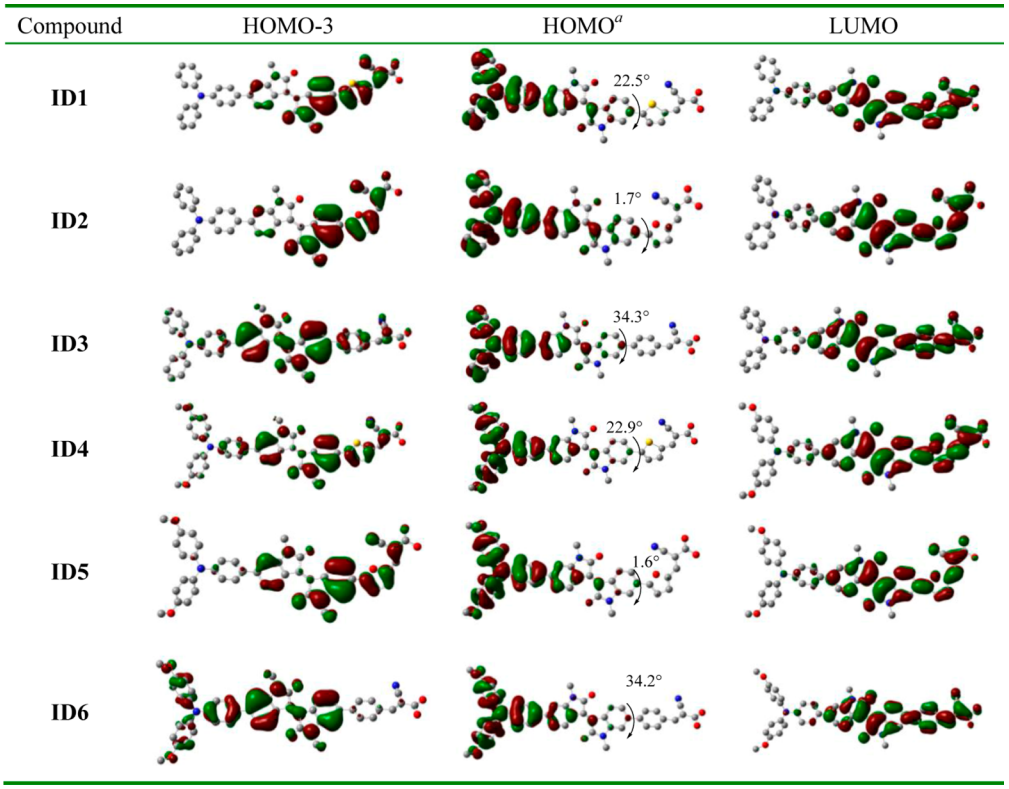

Figure 4. Frontier orbitals of compounds **ID1**−**ID6**, calculated at (isodensity = 0.020 au). Hydrogens are omitted for clarity. The angles in the HOMO structures are dihedral angles between the isoindigo rings and π-spacer near anchoring moiety.

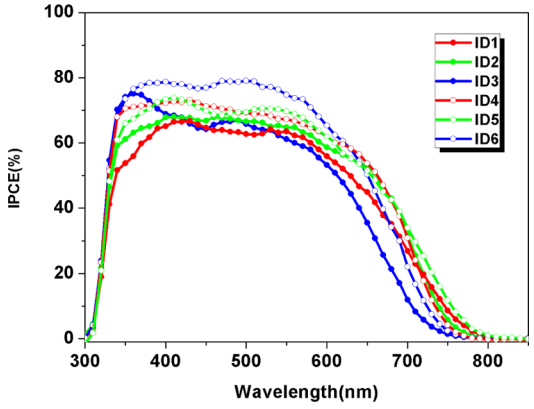

Figure 5. IPCE spectrum for DSSCs sensitized by **ID1**−**ID6**.

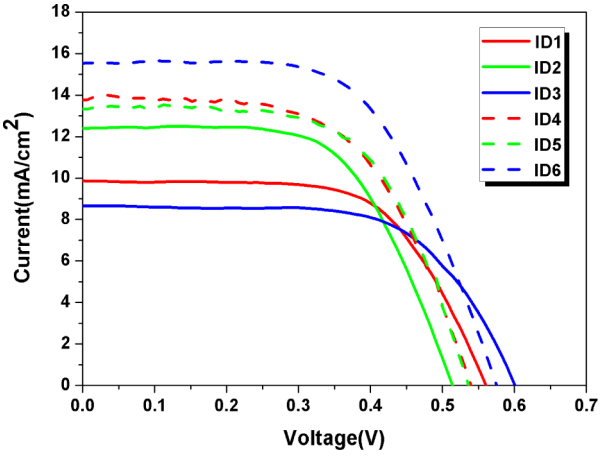

Figure 6. The I−V performance of solar cells sensitized by **ID1**−**ID6** dyes.

ID3. In addition, the open-circuit voltage of six dyes is much lower than that of N719. This outcome may be comprehended to the shorter electron lifetime obtained from electrochemical impedance spectroscopy (EIS shown in Figure 8 and Table 4). From the data of open-circuit voltage (V_{oc}) of **ID1**−**ID3**-based DSSCs, the V_{oc} of **ID3** with benzene ring is better than those of **ID1 and ID2**. Similar to **ID1**−**ID3**, **ID6** performs the best V_{oc} for **ID4**−**ID6**. The introduction of benzene group can lead to reduction of electron recombination and improve V_{oc} due to the relative large dihedral angle between isoindigo ring and benzene-bridged **ID3** and **ID6**. It can be concluded that the dyes contain benzene as the linker exhibits better V_{oc} values for these isoindigo dyes. Finally, the **ID1**−**3**-sensitized solar cells gave a J_{sc} of 9.89, 12.24, and 8.72 mA/cm^2, a V_{oc} of 559, 513, and 596 mV, and a *ff* of 0.64, 0.62, and 0.64, corresponding to an overall conversion efficiency of 3.52, 3.92, and 3.33%, respectively. Under the same condition, the photovoltaic parameters (J_{sc}, V_{oc}, *ff*, and η) of cell sensitized by **ID4**−**ID6** are 13.66 mA/cm^2, 540 mV, 0.59, and 4.36%; 13.27 mA/cm^2, 536 mV, 0.62, and 4.41%; 15.50 mA/cm^2, 574 mV, 0.60, and 5.35%, respectively.

To reduce aggregation, we have codeposited nonchromophoric coadsorbents, such as deoxycholic acid (DCA) or chenodeoxycholic acid (CDCA), onto semiconductor surfaces. Because **ID6** exhibits the best performance among the six dyes studied in this work, we focus on the optimization of **ID6**-based DSSC using coadsorption strategy and the data are summarized in Table 3. Before dipping into dye CH_2Cl_2 solution, TiO_2 films were pretreated with different concentration of CDCA in ethanol solution for 6 h. Figure 7 shows the photovoltaic

dx.doi.org/10.1021/am300925e | ACS Appl. Mater. Interfaces 2012, 4, 4215−4224

Table 3. Photocurrent−Voltage Characteristics of Untreated DSSCs Based on ID1−ID6 and N719 and CDCA with Different Concentrations of 10, 20, and 30 mM Coadsorbed DSSCs Based on ID6[a]

dye	CDCA (mM)	J_{sc} (mA cm^{-2})	V_{oc} (mV)	*ff*	η (%)
ID1	0	9.89	559	0.64	3.52
ID2	0	12.24	513	0.62	3.92
ID3	0	8.72	596	0.64	3.33
ID4	0	13.66	540	0.59	4.36
ID5	0	13.27	536	0.62	4.41
ID6	0	15.50	574	0.60	5.35
	10	14.45	633	0.59	5.41
	20	14.77	644	0.63	5.98
	30	13.61	647	0.62	5.48
N719	0	17.79	718	0.60	7.64

[a]Illumination: 100 mW cm^{-2} simulated AM 1.5 G solar light; electrolyte containing: 0.05 M I_2 + 0.5 M LiI in the mixed solvent of acetonitrile and 3-methoxypropionitrile (7:3, v/v).

Table 4. Parameters Estimated by Ftting the EIS Spectra of the ID1−ID6 Sensitized DSSCs Using the Equivalent Circuit

	CDCA (Mm)	R_S (Ω)	R_{CE} (Ω)	R_{rec} (Ω)	τ_e (ms)
ID1	0	27.4	5.3	9.2	4.6
ID2	0	29.0	6.4	5.6	2.4
ID3	0	26.6	7.2	9.5	5.0
ID4	0	28.6	5.4	8.4	4.3
ID5	0	27.7	4.3	7.7	3.4
ID6	0	30.6	5.1	8.6	4.8
	20	28.9	8.9	25.4	10.1

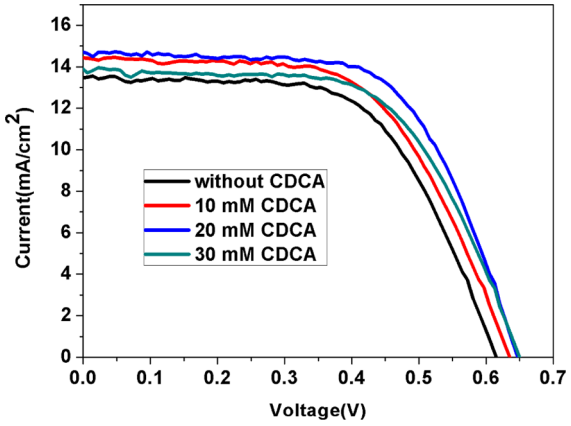

Figure 7. *I*−*V* curves of cells based on **ID6** coabsorption with different concentration (0, 10, 20, and 30 mM) CDCA.

performance of **ID6**-based DSSCs coadsorbed with 10, 20, 30 mM CDCA using 0.05 M I_2, 0.5 M LiI as redox electrolyte. In general, the V_{oc} values increased (from 575 mV to 633, 644, and 647 mV) when the concentration of CDCA increased (from 0 to 10, 20, and 30 mM). This indicates that the injection of coadsorbent CDCA can reduce the electron recombination, extend the electron lifetime, and lead to better open-circuit voltage and efficiency. The short-circuit current of **ID6** reduced (from 15.50 mA/cm^2 to 14.45, 14.77, and 13.61 mA/cm^2) under the same condition. This may be derived from the decrease of the dye load. CDCA with −COOH group takes the place of dye on the surface of TiO_2 film. When the concentration of CDCA increased from 0 mM to 10 mM and 20 mM, the raise of V_{oc} can counterbalance the decrease of photocurrent. Finally the photoelectron conversion efficiency increased from 5.35 to 5.41 and 5.98%. The increase in V_{oc} cannot balance the photocurrent's reduction and the efficiency flowed to 5.48% when the concentration of CDCA increased to 30 mM. The **ID6**-based DSSCs gave the best performance of 5.98% using 20 mM CDCA as coadsorbent.

Electrochemical Impedance Spectroscopy (EIS). EIS was employed to study the electron recombination in DSSCs based on these **ID1−ID6** dyes under −0.70 V bias applied voltage in the dark. The Nyquist plot (a), Bode plot (b) and equivalent circuit (c) are shown in Figure 8. Some important

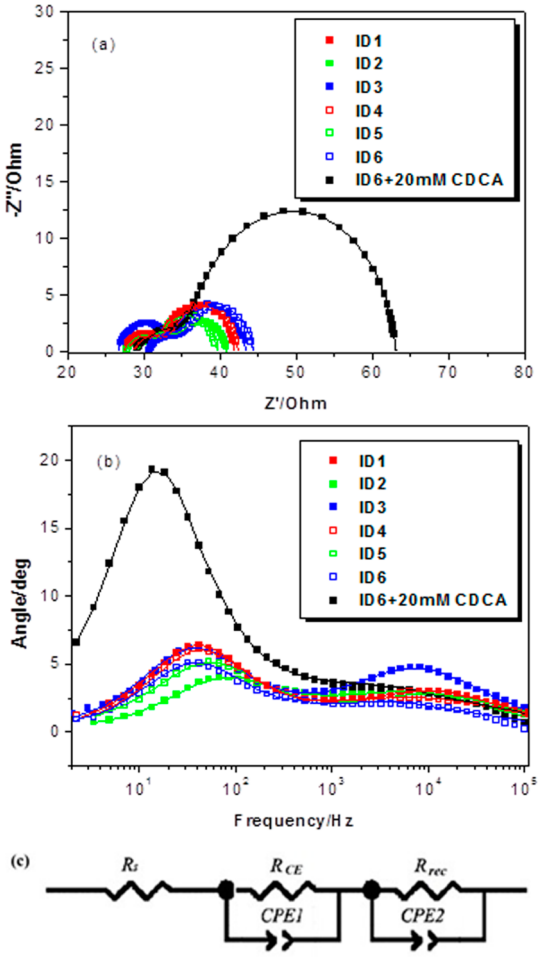

Figure 8. Impedance spectra (a) Nyquist plots and (b) Bode phase plots and (c) equivalent circuits for DSSCs based on **ID1−ID6** dyes measured at −0.70 V bias in the dark. The lines of a and b show theoretical fits using the equivalent circuits c.

parameters can be obtained by fitting the EIS spectra with an electrochemical model.[33] The R_S, R_{rec}, and R_{CE} represent series resistances, charge transfer resistances at the dye/TiO_2/electrolyte interface and counter electrode (CE), respectively. The reaction resistance of the DSSCs consisting of Pt/electrolyte and TiO_2/dye/electrolyte interface based on **ID1−ID6** were tested by software (ZSimpWin) with an equivalent circuit. The series resistance (R_S) and electrolyte reduction resistance (R_{CE}) corresponding to the first semicircle showed almost the same value in the six dyes-based DSSCs due to the same electrode material and same electrolyte, and the R_{rec} is corresponding to the middle semicircle (Figure 8). From the EIS measurements, the electron lifetime (τ_e) expressing the

electron recombination between the electrolyte and TiO_2 was calculated following the literature.[34]

Figure 8b shows the Bode plots of DSSCs based on **ID1**−**ID6**. All EIS Bode plots exhibit two peak features for the frequency investigated. The one at higher frequencies corresponds to the charge transfer at the Pt/electrolyte interface and the other one at lower frequencies corresponds to the charge transfer at TiO_2/dye/electrolyte interface, which is related to the charge recombination rate and whose reciprocal is associated with the electron lifetime.[35] In Figure 8, the low-frequency peak of **ID6** shows a lower frequency than those of **ID1**−**ID5**, indicating that **ID6**-based DSSCs has longer electron lifetime, which leads to lower rate of charge recombination. The electron lifetime values of **ID1**−**ID6** are 4.6, 2.4, 5.0, 4.3, 3.4, and 4.8 ms, respectively, likewise supporting the observed shift in the V_{oc} value under standard global AM 1.5 solar light condition. Among **ID1**−**ID6**, **ID6**-based DSSCs shows the highest V_{oc} because of the slight blocking effect of methoxy group and benzene ring, as a result of enhanced electron lifetime. After cosensitized with CDCA, the low-frequency peak of **ID6** shows much lower frequency than before, and it indicates that 20 mM CDCA cosensitized **ID6**-based cell has longer electron lifetime, which leads to lower rate of charge recombination and thus improved V_{oc}.

CONCLUSIONS

In conclusion, we have designed and synthesized six new D-A-π-A sensitizers **ID1**−**ID6**, with triarylamine as the electron donor, isoindigo as a auxiliary electron withdrawing unit, thiophene, furan, and benzene as the linker and cyanoacrylic acid as the acceptor moiety. The results based on photovoltaic experiments showed that the introduction of methoxy triphenylamine group as the electron-donor brought about improved photovoltaic performance for isoindigo dyes. Co-adsorption of CDCA can decrease the dye aggregates and suppress charge recombination, leading to the increasing electron lifetime and thus photovoltage. The best overall light to electricity conversion efficiency of 5.98% (J_{sc} = 14.77 mA cm^{-2}, V_{oc} = 644 mV, ff = 0.63) under simulator AM 1.5 solar light irradiation (100 mW cm^{-2}) with a 20 mM CDCA coadsorbed DSSC based on **ID6** was obtained. The results indicate that the drawback of these isoindigo-based DSSCs is the low V_{oc}, so much higher efficiency can be expected if we can improve the V_{oc} significantly (e.g., >0.75 V). Our future work will focus on further molecular engineering to fine-tune the energy levels of the dye toward higher V_{oc} and broader spectra.

AUTHOR INFORMATION

Corresponding Author

*E-mail: jlhua@ecust.edu.cn. Fax: 86-21-64252758. Tel: 86-21-64250940.

Author Contributions

†These authors contributed equally to this work.

Notes

The authors declare no competing financial interest.

ACKNOWLEDGMENTS

This work was supported by NSFC/China (2116110444, 21172073 and 21190033), National Basic Research 973 Program (2011CB808400), the Fundamental Research Funds for the Central Universities (WJ0913001 and WJ1114050) and Ph. D. Programs Foundation of Ministry of Education of China (20090074110004).

REFERENCES

(1) Grätzel, M. *Nature* **2001**, *414*, 338−344.
(2) Hagfeldt, A.; Boschloo, G; Sun, L. C.; Kloo, L.; Pettersson., H. *Chem. Rev.* **2010**, *110*, 6595−6663.
(3) Grätzel, M. *Acc. Chem. Res.* **2009**, *42*, 1788−1798.
(4) Mishra, A.; Fischer, M. K.; Bäuerle, P. *Angew. Chem., Int. Ed.* **2009**, *48*, 2474−2499.
(5) Shrestha, M.; Si, L. P.; Chang, C. W.; He, H. S.; Sykes, A.; Lin, C. Y.; Diau, E. W.-G. *J. Phys. Chem. C* **2012**, *116*, 10451−10460.
(6) Vercelli, B.; Zotti, G.; Berlin, A. *ACS Appl. Mater. Interfaces* **2012**, *4*, 3233−3238.
(7) Wu, W. J.; Guo, F. L.; Li, J.; He, J. X.; Hua, J. L. *Synth. Metal* **2010**, *160*, 1008−1014.
(8) Karlsson, K. M.; Jiang, X.; Eriksson, S. K.; Gabrielsson, E.; Rensmo, H.; Hagfeldt, A.; Sun, L. C. *Chem.—Eur. J.* **2011**, *17*, 6415−6424.
(9) Funabiki, K.; Mase, H.; Saito, Y.; Otsuka, A.; Hibino, A.; Tanaka, N.; Miura, H.; Himori, Y.; Yoshina, T.; Kubota, Y.; Matsui, M. *Org. Lett.* **2012**, *14*, 1246−1249.
(10) Wang, Z. S.; Cui, Y.; Hara, K.; Dan-oh, Y.; Kasada, C.; Shinpo, A. *Adv. Mater.* **2007**, *19*, 1138−1141.
(11) Chen, Y. S.; Li, C.; Zeng, Z. H.; Wang, W. B.; Wang, X. S.; Zhang, B. W. *J. Mater. Chem.* **2005**, *15*, 1654−1661.
(12) Akhtaruzzaman, M.; Islam, A.; Yang, F.; Asao, N.; Kwon, E.; Singh, S. P.; Han, L. Y.; Yamamoto, Y. *Chem. Commun.* **2011**, *47*, 12400−12402.
(13) Qu, S. Y.; Wu, W. J.; Hua, J. L.; Kong, C.; Long, Y. T.; Tian., H. *J. Phys. Chem. C* **2010**, *114*, 1343−1349.
(14) He, J. X.; Guo, F. L.; Wu, W. J.; Li, X.; Yang, J. B.; Hua, J. L. *Chem.—Eur. J.* **2012**, *18*, 7903−7915.
(15) Mao, J. Y.; Guo, F. L.; Ying, W. J.; Wu, W. J.; Li, J.; Hua, J. L. *Chem.—Asian J.* **2012**, *7*, 982−991.
(16) Li, W. Q.; Wu, Y. Z.; Zhang, Q.; Tian, H.; Zhu, W. H. *ACS Appl. Mater. Interfaces* **2012**, *4*, 1822−1830.
(17) Pei, K.; Wu, Y. Z.; Zhang, Q.; Chen, B; Tian, H.; Zhu, W. H. *Chem.—Eur. J.* **2012**, *18*, 8190−8200.
(18) Weea, X. K.; Yeo, W. K.; Zhang, B.; Tan, V. B. C.; Lim, K. M.; Tay, T. E.; Go, M. *Bioorg. Med. Chem.* **2009**, *17*, 7562−7571.
(19) Mei, J. G.; Graham, K. R.; Stalder, R.; Reynolds, J. R. *Org. Lett.* **2010**, *12*, 660−663.
(20) Zhang, G. B.; Fu, Y. Y.; Xie, Z. Y.; Zhang, Q. *Macromolecules* **2011**, *44*, 1414−1420.
(21) Liu, B.; Zou, Y. P.; Peng, B.; Zhao, B.; Huang, K. L.; He, Y. H.; Pan, C. Y. *Polym. Chem.* **2011**, *2*, 1156−1162.
(22) Wang, E. G.; Ma, Z. F.; Zhang, Z.; Henriksson, P.; Inganäs, O.; Zhang, F. L.; Andersson, M. R. *Chem. Commun.* **2011**, *47*, 4908−4910.
(23) Wang, E. G.; Ma, Z. F.; Zhang, Z.; Vandewal, K; Henriksson, P.; Inganäs, O.; Zhang, F. L.; Andersson, M. R. *J. Am. Chem. Soc.* **2011**, *133*, 14244−14247.
(24) Qin, C. J.; Peng, W. Q.; Zhang, K.; Islam, A.; Han, L. Y. *Org. Lett.* **2012**, *14*, 2532−2535.
(25) Chou, M. Y.; Leung, M.-K.; Su, Y. O.; Chiang, C. L.; Lin, C. C.; Liu, J. H.; Kuo, C. K.; Mou, C. Y. *Chem. Mater.* **2004**, *16*, 654−661.
(26) Koumura, N.; Wang, Z. S.; Miyashita, M.; Uemura, Y.; Sekiguchi, H.; Cui, Y.; Mori, A.; Mori, S.; Hara, K. *J. Mater. Chem.* **2009**, *19*, 4829−4834.
(27) Lin, L. Y.; Tsai, C. H.; Wong, K. T.; Huang, T. W.; Hsieh, L.; Liu, S. H.; Lin, H. W.; Wu, C. C.; Chou, S. H.; Chen, S. H.; Tsai, A. I. *J. Org. Chem.* **2010**, *75*, 4778−4785.
(28) Li, R. Z.; Shi, D.; Zhou, D. F.; Cheng, Y. M.; Zhang, G. L.; Wang, P. *J. Phys. Chem. C* **2009**, *113*, 7469−7479.
(29) Frisch, M. J.; Trucks, G. W.; Schlegel, H. B.; Scuseria, G. E.; Robb, M. A.; Cheeseman, J. R.; Scalmani, G.; Barone, V.; Mennucci, B.; Petersson, G. A.; Nakatsuji, H.; Caricato, M.; Li, X.; Hratchian, H. P.; Izmaylov, A. F.; Bloino, J.; Zheng, G.; Sonnenberg, J. L.; Hada, M.; Ehara, M.; Toyota, K.; Fukuda, R.; Hasegawa, J.; Ishida, M.; Nakajima,

T.; Honda, Y.; Kitao, O.; Nakai, H.; Vreven, T.; Montgomery, J. A.; Peralta, J. E.; Ogliaro, F.; Bearpark, M.; Heyd, J. J.; Brothers, E.; Kudin, K. N.; Staroverov, V. N.; Kobayashi, R.; Normand, J.; Raghavachari, K.; Rendell, A.; Burant, J. C.; Iyengar, S. S.; Tomasi, J.; Cossi, M.; Rega, N.; Millam, J. M.; Klene, M.; Knox, J. E.; Cross, J. B.; Bakken, V.; Adamo, C.; Jaramillo, J.; Gomperts, R.; Stratmann, R. E.; Yazyev, O.; Austin, A. J.; Cammi, R.; Pomelli, C.; Ochterski, J. W.; Martin, R. L.; Morokuma, K.; Zakrzewski, V. G.; Voth, G. A.; Salvador, P.; Dannenberg, J. J.; Dapprich, S.; Daniels, A. D.; Farkas, O.; Foresman, J. B.; Ortiz, J. V.; Cioslowski, J.; Fox, D. J. *Gaussian 09, Revision A.02*; Gaussian, Inc.: Wallingford, CT, 2009.

(30) Becke, A. D. *J. Chem. Phys.* **1993**, *98*, 1372−1377.

(31) Lynch, B. J.; Fast, P. L.; Harris, M.; Truhlar, D. G. *J. Phys. Chem. A* **2000**, *104*, 4811−4815.

(32) Cossi, M.; Barone, V. *J. Chem. Phys.* **2001**, *115*, 4708−4717.

(33) Fabregat-Santiago, F.; Garcia-Belmonte, G.; Mora-Sero, I.; Bisquert, J. *Phys. Chem. Chem. Phys.* **2011**, *13*, 9083−9118.

(34) Zou, L. C.; Hunt, C. *J. Electrochem. Soc.* **2009**, *156*, C8−C15.

(35) Lin, L. Y.; Tsai, C. H.; Wong, K. T.; Huang, T. W.; Hsieh, L.; Liu, S. H.; Lin, H. W.; Wu, C. C.; Chou, S. H.; Chen, S. H.; Tsai, A. I. *J. Org. Chem.* **2010**, *75*, 4778−4785.